PROCEEDINGS, Thirtieth Workshop on Geothermal Reservoir Engineering
Stanford University, Stanford, California, January 31-February 2, 2005
SGP-TR-176

FOUR DIMENSIONAL VELOCITY STRUCTURE OF THE SOULTZ-SOUS-FÔRETS GEOTHERMAL RESERVOIR DURING THE 2000 AND 2003 STIMULATIONS

J. Charléty[1], N. Cuenot[1], C. Dorbath[1,2], L. Dorbath[1,2]

[1)] EOST-ULP 5, rue rené Descartes, Strasbourg, France
[2)] IRD, Toulouse, France
e-mail: jean.charlety@eost.u-strasbg.fr

ABSTRACT

The stimulation of 2000 and 2003 carried out on the HDR site of Soultz-sous-Forêts (Alsace, France) have generated a continuous, small magnitude seismic activity. For each experiment, a seismological network composed of about 25 stations were installed by the Ecole et Observatoire des Sciences de la Terre (EOST). More than 3500 seismic events has been pointed and located in both cases.

In order to estimate the variation of the physical properties of the reservoir due to the fluid circulation, we have performed a four dimensional tomography: the 3D velocity structure for different time windows. The whole data set has been apportioned into different temporal sets with a fixed number of events. We use the tomographic algorithm of Thurber (1983) for 2000 and a new, more accurate method for the set of 2003 based on a double difference tomography (Zhang & Thurber, 2003). The latter method gives a good resolution within the reservoir volume and allows a relatively good resolution in the vicinity of this volume. It enlights the velocity structure variation in the reservoir all along the stimulation.

In this study, we propose a dicussion based on the variation of the velocity in time during each stimulation and a comparison of the variation of the velocity in 2000 and 2003. This analysis allows us to appreciate the volume of influence of the hydraulic activity and points out the effect of the water circulation on the reservoir properties.

INTRODUCTION

In 2000 and 2003, massive hydraulic stimulations were carried out at the geothermal Hot Dry Rock site at Soultz-sous-Fôrets, France. These stimulations were performed in the 5000 m deep wells, in the crystalline basement. The objective was to create a dense network of enhanced permeability fractures, which would form the heat exchanger. The deformation entailed by the injection of fluid caused a microseismic activity.

Network

In 2000, the seismic network comprises around 20 stations divided into a telemetered network with eight vertical sensors, a network composed by six autonomous three-component sensors, and three four-component sensors deployed in wells at around 1.5 km depth. The latter is owned by the EEIG "Heat mining". The network changed in 2003.

Since the begining of 2003, a field-wide permanent seismic network has been in place and was run by a team at the Institut de Physique du Globe from Strasbourg (France). The network comprises 9 stations and covers the geothermal reservoir. The sampling rate is 6.66 ms. The frequency band of the acquisition is from 1 to 48 Hz. Three stations have three-component sensors and the others only vertical ones. Fourteen additional seismometers have supplemented the permanent network. Six stations have three-component sensors and the others only vertical ones. The three-components sensors have the same caracteristics as the permanent network. The vertical seismometers have a sampling rate of 5.55 ms and the frequency band is from 1 to 60 Hz.

Hydraulic Stimulations

The aim of the stimulation of 2000 was to improve the hydraulic connexion between the well GPK2 and the endemic fracture system. It started the 30th of june and lasted almost seven days. The flow-rate followed a step-wise strategy. The first step lasted less than one day with a flow-rate of 30 l.s^{-1}; the second lasted more than one day with a flow-rate of 40 l.s^{-1}; the third part lasted around 4 days with a flow-rate of 50 l.s^{-1} (figure 1 top).

The aims for the 2003 stimulation did not change but it concerned the well GPK3: improvement of its injectivity and the relatedness between the two wells. It started the 27th of may and lasted 11 days. The fluid injection strategy was more complex than in 2000.

The flow-rate has been up to 93 $l.s^{-1}$ on a very short period (some hours) (figure 1 bottom).

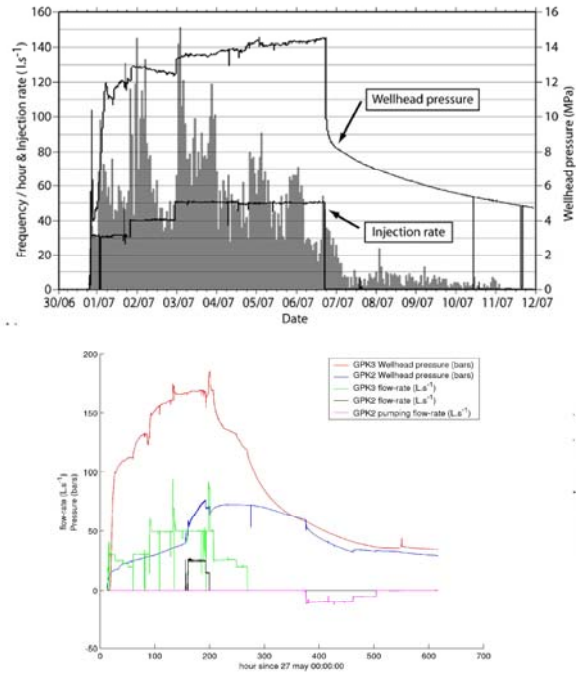

Figure 1 Injection strategy for 2000 (top) and 2003 (bottom). Top: are represented the wellhead pressure and the injection rate. In grey appears the number of seismic events per hour detected on the surface seismic network. Bottom: the wellhead pressure of GPK3 (red) and GPK2 (blue), and the flow-rate in GPK3 (green) and GPK2 (black and purple) are represented. The purple curve corresponds to the pumping strategy in GPK2.

METHOD

Data

The data from all the seismic sensors have been picked and used for the tomography. In 2000, more than 10 000 events has been recorded. More than 7000 events have been used to perform the tomography. The P and S arrival time have been manually picked (Cuenot et *al.*, 2005). For 2003 an automatic detection algorithm has been used. The detection has been made for more than 6000 events. The data has been automatically picked by a AR-AIC algorithm (Leonard and Kennett, 1999). The tomography has been achieved with about 2250 events. Concerning the S wave arrival time picks, where shear wave birefringence was noted, the earliest S arrival was picked. S waves were picked only on horizontal components. A first location of the events was made by a hypoinverse-like algorithm with a 8 tabular layer model. This model is based on the information derived from different log-data.

Tomography

The tomography used is based on the program simulps (Thurber, 1983). Simulps uses an iterative, damped least squares method to invert arrival times, simultaneously estimating earthquake locations and the three-dimensional V_p and V_p/V_s fields. The velocity structures are parameterized by values defined at the nodes of a three-dimensional grid, between which the V_p and V_p/V_s values are assumed to follow trilinear functions.

Zhang and Thurber (2003) have developed a new method that combines both absolute and relative arrival time data. The method determines an 3D velocity model jointly with absolute and relative event locations. They developed a double difference (DD) tomography code tomoDD based on the DD location code hypoDD (Waldhauser, 2001). In their simultaneous inversion for velocity structure and event locations, velocity anomalies are constrained by seeking a first-order smooth model. The same smoothing weight is applied to the horizontal and vertical regions. This smoothing regularization should provide a minimum-feature model that contains only as much as structure as can be resolved above the estimated level of noise in the data.

The two different types of data are combined into one system thanks to a hierarchical weighting scheme during the inversion. We start the inversion by applying greater weight to the absolute catalog data (1 for absolute data, 0.1 for differential catalog data) to establish the large scale result. The differential catalog data are weighted more to refine the event locations and the velocity structure near the source regions (1 for differential data, 0.1 for absolute catalog data). Then we finish the inversion by weighting equivalently both catalogs. For each step, two iterations are performed. The system is solved by a LSQR algorithm for the damped least-square problem.

The tomography method has changed between 2000 and 2003. In 2000, we used the simulps methodology while in 2003, tomoDD is used. As for both year the number of events is important, we decided to divide them into temporal sets so that the evolution of the velocity structure can be imaged. For 2000, a set of data is composed by 500 events (table 1). In 2003, as a differential catalog data is also used, the number of events per set is set to 250 (table2). In 2003 the number of events per set has been chosen in order to appreciate the effect of each injection stage: increase or decrease of the flow-rate, dual injection (injection in GPK2 and GPK3), shut-in.

Sample	Duration	Number of arrival times	
		P-wave	S-wave
1	30/06/00 @ 19h15 01/07/00 @ 08h16	5739	2263
2	01/07/00 @ 08h17 01/07/00 @ 19h46	5840	2140
3	01/07/00 @ 19h46 02/07/00 @ 03h18	5198	2305
4	02/07/00 @ 03h21 02/07/00 @ 12h12	5098	2488
5	02/07/00 @ 12h17 03/07/00 @ 04h26	5044	1707
6	03/07/00 @ 04h36 03/07/00 @ 13h58	5428	1875
7	03/07/00 @ 13h59 03/07/00 @ 20h22	5933	2523
8	03/07/00 @ 20h23 04/07/00 @ 04h23	5606	2373
9	04/07/00 @ 04h26 04/07/00 @ 17h09	4940	2111
10	04/07/00 @ 17h18 05/07/00 @ 02h55	5076	1965
11	05/07/00 @ 03h00 05/07/00 @ 15h41	5568	2290
12	05/07/00 @ 15h43 06/07/00 @ 01h04	6336	2757
13	06/07/00 @ 01h07 06/07/00 @ 16h30	6038	2955
14	06/07/00 @ 16h32 11/07/00 @ 05h58	6422	2989

Table 1: Detail of each set for the 2000 tomography with their duration and number of available P- and S-wave arrivals.

Sample	Duration	Number of arrival times	
		P-wave *dp data*	S-wave *ds data*
1	27/05/03 @ 18h37 30/05/03 @ 23h54	4246 *42936*	1773 *19936*
2	30/05/03 @ 23h54 01/06/03 @ 03h42	4118 *40608*	1759 *19563*
3	01/06/03 @ 03h42 02/06/03 @ 08h04	4202 *42635*	1796 *19703*
4	02/06/03 @ 08h04 03/06/03 @ 16h56	4514 *44566*	1795 *19652*
5	03/06/03 @ 16h56 04/06/03 @ 16h41	4559 *43545*	1983 *20939*
6	04/06/03 @ 16h41 05/06/03 @ 20h28	4474 *42564*	1982 *20835*
7	05/06/03 @ 20h28 07/06/03 @ 12h33	4473 *41080*	1938 *19686*
8	07/06/03 @ 12h33 09/06/03 @ 23h22	4435 40100	1927 18733
9	09/06/03 @ 23h22 19/06/03 @ 19h29	4699 *42648*	2002 *19729*

Table 2: Events samples for the 2003 tomography with their corresponding duration and number of available P- and S-wave arrivals for the absolute and relative catalog.

The grid covered all the area determined by the location of the seismic sensors. As the rays intercept each other in the volume of the reservoir the resolution of the tomography is good only at the depth of the injection. Thus the grid has been refined in this part.

Depth (km)	V_p $(km.s^{-1})$	V_p/V_s
-15	1,5	2,14
0	1,85	2,14
0,8	2,87	2,14
1,6	5,8	1,75
2,6	5,82	1,75
3,6	5,85	1,75
4,6	5,87	1,75
5,6	5,9	1,75
6,6	5,92	1,75
15	5,95	1,75

Table 3: Initial velocity model for the tomography of 2000 and 2003. The depth is positive below sea level. The first and last layer are used as buffer.

The initial model for both tomography is the same for each set of data and tomography (table 3).

The tomoDD code is similar to simulps if the relative catalog is not taking into account in the inversion (weight is put to 0). We have tested this approach on the first set in order to appreciate the difference between the methods. The difference in the results are quite small and it appears that the velocity values for the simulps inversion is almost always greater.

Other tests have been made. The 3D velocity model obtained is almost insensitive to starting model, event set and inversion strategy.

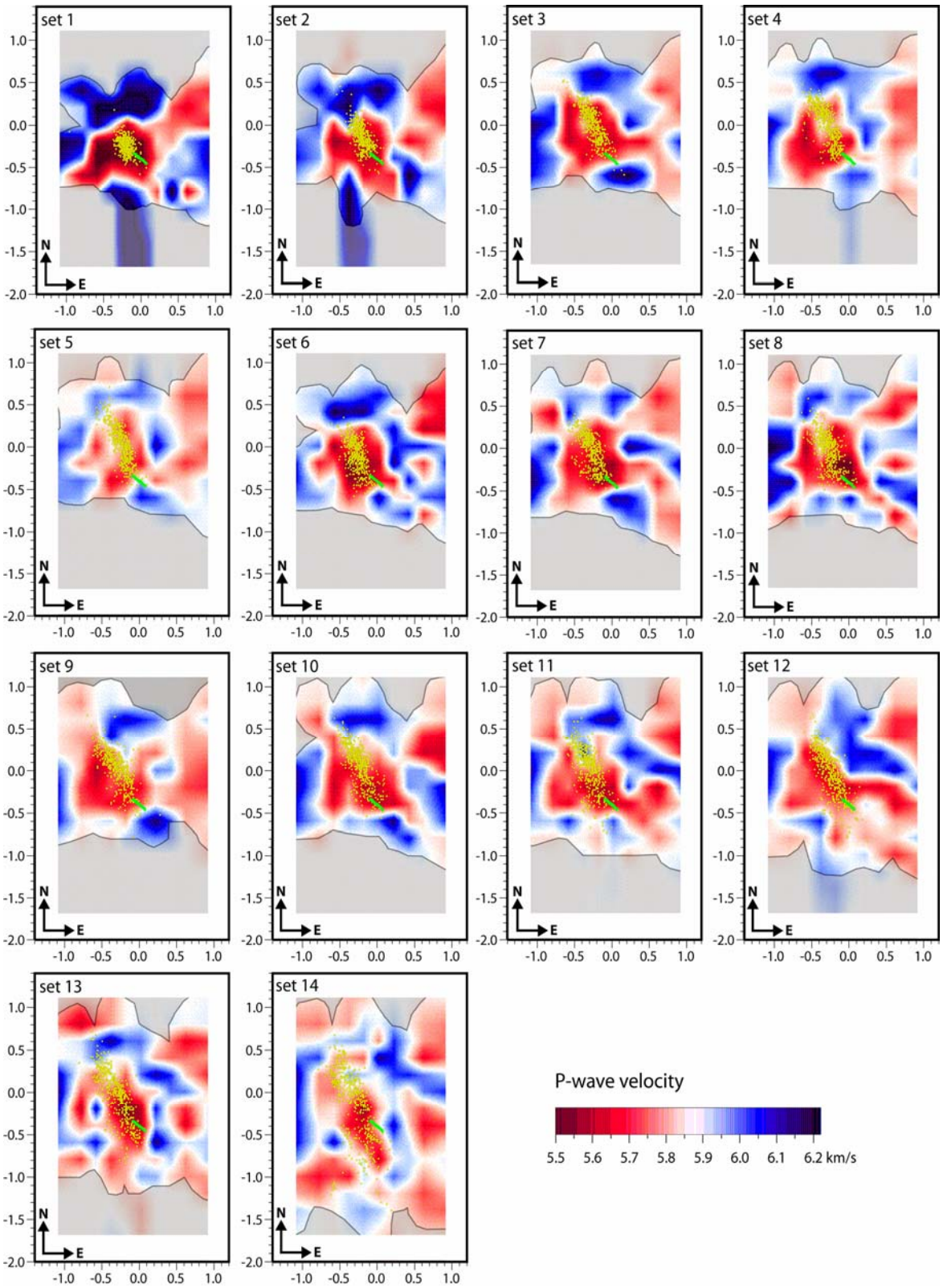

Figure 2: Evolution of the P-wave seismic velocity at 4.6 km depth during the 2000 stimulation test. Images are in chronological order from set 1 to set 14. Yellow dots represent the 500 events used in the computation for each subfigure. The green line corresponds to the open-hole section of the injection well GPK2. Grey areas do not have to be considered as they define zones of poor resolution.

RESULTS

The velocity structure of each tomography is corrupted by the lack of knowledge of the velocity model before the stimulation. The region is seismically quiet so that no natural seismicity has been localy recorded prior to the hydraulic experiments. It is also obvious that the seismicity is linked with the injection of fluid. This tomography could have given us essential information on the steady state in the reservoir. Nevertheless we described the global evolution of the velocity structure as in shape and value. We consider that as the treatment of each set is exactly the same the variation from one set to an other is meaningful.

Temporal evolution of the 2000 V_p velocity structure

A sequence of fourteen successive images was computed to observe the evolution of the V_P velocity in the geothermal reservoir (figure 2). On each plot are represented the corresponding 500 events used for the calculation to outline the shape and position of the microseismic cloud at that time. The trajectory of the open-hole section of the well GPK2 is also indicated. Hatchured zones do not have to be considered as they correspond to low-resolution areas.

Figure 2 presents the temporal evolution of the velocity structure at a depth of 4.6 km, corresponding to the location of the stimulated rock volume. Set 1 is calculated using the 500 first events of the stimulation. The dark red colour clearly denotes a significant low-velocity anomaly: the plotted microseismic cloud indicates that this anomaly corresponds to the geothermal reservoir. It is difficult to interpret this first result, as we cannot compare the present situation to that before the beginning of the injection: is the anomaly directly due to the start of the stimulation or does it actually exist before? Set 2 to set 5 show a slight increase of the velocity from 5.6 $km.s^{-1}$ to about 5.8 $km.s^{-1}$. An interesting feature appears between set 5 and set 6: on the figure 2 one can notice the reappearance of the dark red colour at the place of the geothermal reservoir, indicating a sudden decrease of the P-velocity of about 0.2 $km.s^{-1}$. Then, until the end of the recording period, velocity slowly increases in the same way as at the beginning of the experiment. What does induce the quick decrease of the velocity? It appears from the injection curve that set 6 contains events occurred just after the increase of the injection rate to 50 $l.s^{-1}$. We did not indeed observe such a variation between set 3 and set 4 although the injection rate was incremented from 30 $l.s^{-1}$ to 40 $l.s^{-1}$ between these periods. Nevertheless, we found some clear correlations between the increase of injection rate up to 50 $l.s^{-1}$ and change in the hydrological parameters and seismic activity evolution that we cannot observe after the augmentation from 30 $l.s^{-1}$ to 40 $l.s^{-1}$.

Temporal evolution of the 2003 V_P and V_S velocity structure

A sequence of nine successive images was computed to observe the evolution of the V_P velocity in the geothermal reservoir. On the figure 3, are represented for each set the seismicity in black dot and a white line demarcating the region where the number of rays per node is greater than or equal to 50. This number of rays commonly determine the part of the figure where the inversion resolution is good. The code tomoDD does not compute the resolution as the least square theory allows.

For the P wave velocity (figure 3), the views represent the evolution of the absolute velocity on horizontal plane at 4.6 km depth. On the first set, a large low wave velocity area dominates the first order spatial variation in V_p structure. This area is located around the well GPK3 near the coordinate (0;-1). This set is associated with the period where the flow-rate is not higher than 30 $l.s^{-1}$. Set 2 corresponds with an increase of the flow rate to 50 $l.s^{-1}$. We observe that the velocity decreases and that the region affected by this change grows. Then in the set 4 the velocity tends to slightly increase. The injection in both GPK2 (-0.2;-0.4) and GPK3 makes increase the velocity and grow the affected area on the northwestern part. Set 5 corresponds to the end of the dual injection. We note that the velocity increases around GPK3 and decreases around GPK2. Set 6 and 7 coincide with the end of the injection in GPK3. We can notice that the velocity remains nearly the same but the location of the maximum velocity region near GPK2 migrates to the northwestern part of the reservoir and that it appears a region southward of GPK3 where the velocity increases. In the set 8 and 9, the low velocity zone continues its migration toward the northwest and the south away from the injection point. The set 9 corresponds to a active period since, for accelerating the pressure decrease, a production strategy in GPK2 has been decided.

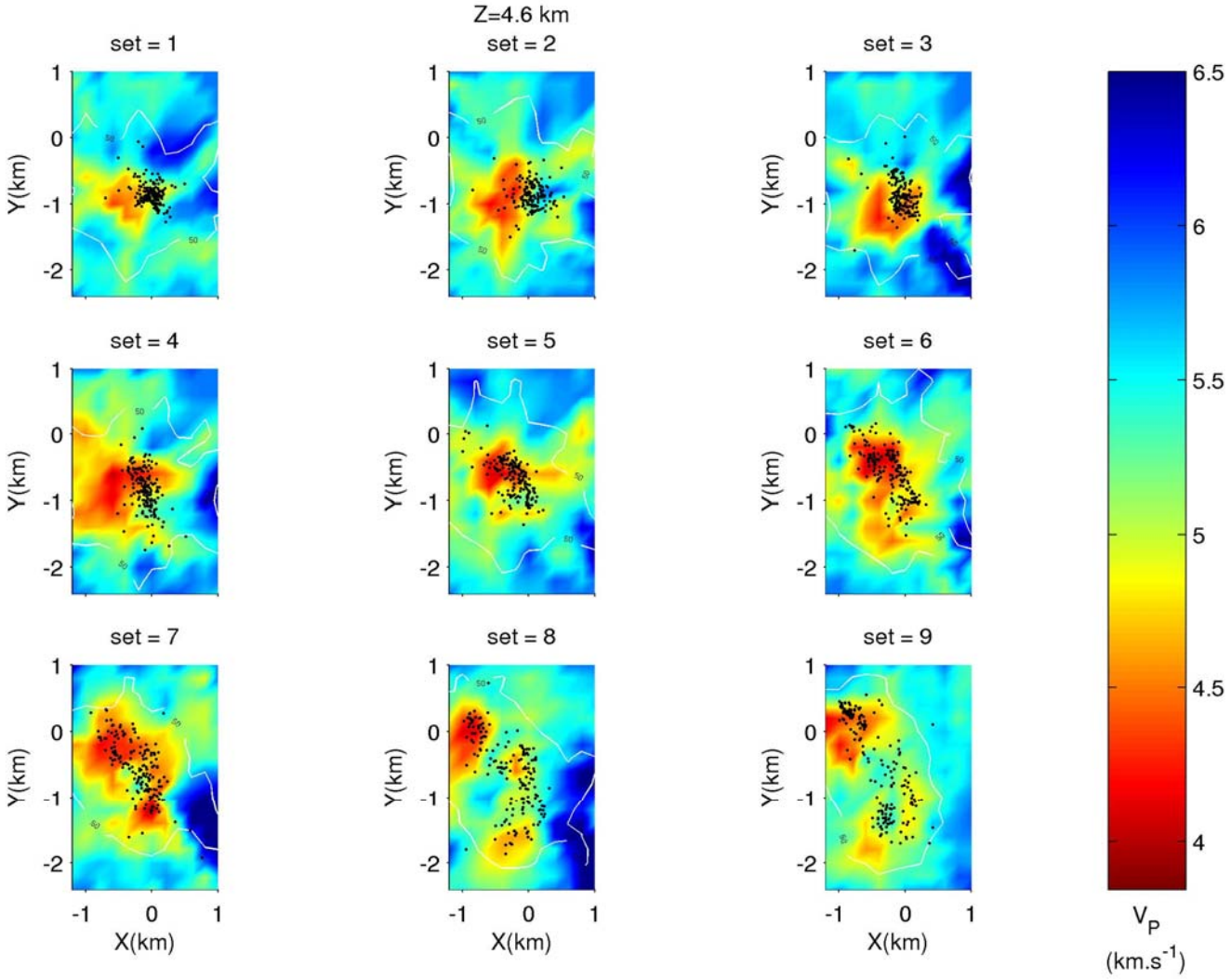

figure 3: Evolution of the P-wave seismic velocity at 4.6 km depth during the 2003 stimulation test. Images are in chronological order from set 1 to set 9. Black dots represent the 250 events used in the computation for each subfigure. The white line demarcates the zone in which the number of rays per node if greater than or equal to 50, supposed to be the good resolution area. North is directed toward positive Y while the East is toward positive X. GPK3 is around (0,-1) and GPK2 (-0.2,-0.5).

INTERPRETATION AND CONCLUSION

The relation between flow-rate change and the velocity variation is clear for both experiment. In 2000, a difference of behaviour from the geothermal reservoir appears between the flow-rate of 30-40 l.s^{-1} and 50 l.s^{-1}. Actually, the decrease of the velocity is higher for the maximum flow-rate. This observation can also be made for 2003. Moreover for the last experiment the effect of the dual injection (injection in both well GPK2 and GPK3) appears clearly on the velocity of the P wave.

Factors that affect V_p include porosity (Wyllie *et al.*, 1956, 1958), pore pressure, partial saturation (Nur and Simmons, 1969), phase transition (Ito *et al.*, 1979) and temperature.

The correlation between the velocity decrease and the flow-rate means that a possible mechanism for the velocity variation is the increase of the pore pressure and/or the porosity, which both phenomenon entail a decrease of the velocity for P wave. The schematic model for this mechanism is an increase of the pressure near the well caused by the injection. This overpressure creates microcracks through which the fluid can migrate. The microcracking creates porosity and the fluid penetration in the rock mass increase the pore pressure. The effect of the pore pressure depends strongly on the saturation of the medium. Then the slow increase of the velocity afterwards can be due to the effects of the cooling of the medium due to the injected fresh fluid and the increase of the saturation of the medium. Both mechanisms make the velocity to increase. The direction of propagation northwest-

southeast corresponds to the direction of regional maximum horizontal stress. This direction has been determined (Tenzer *et al.*, 1991; Rummel and Baumgärtner, 1991; Klee and Rummel, 1993; Benderitter and Elsass, 1995; Helm, 1996) several times in the Upper Rhine Graben region.

In 2003 we note that the northwestern part of the reservoir has still a low velocity after the shut-in. In this region, the largest seismic events have occured in 2000 and in 2003. The set 8 and 9 which correspond to the period after the shut-in show clearly this feature. The decrease of the velocity is due to either the porosity or the pore pressure. Therefore it could be guessed two scenarii. The first one considers that the fluid is led to this region for some reasons so that a large part of the injected fluid remains in this area. The mechanism to invoke is so the pore pressure. The second scenario considers that as the region is submitted to a seismic activity of large magnitude (up to 3 in duration magnitude), the porosity increased and thus the P wave velocity decrease.

The tomography of 2003 allows to observe that after the hydraulic activity, the medium returns to a kind of equilibrium state. It demonstrates that the medium is perturbed by the injection and permit to consider that the first image (set 1) is fully a consequence of the injections.

The tomography used either in 2000 or in 2003 relocate the seismic events in the 3D velocity model. This relocation refine the error in latitude, longitude and depth so that they are around 20 to 30 meters. In 2003 the relocation of the seismic event points out the relation that exists between the seismic activity and the natural endemic fractures. The figure 4 shows the relocation of the 250 first events corresponding to the first set. The fracture represented has been imaged by UBI and the characteristic of the plane has been determined by Dezayes *et al.* (2004). This fracture absorbed around 80 % of the fluid injected as determined by a flow-log. The weakening of the fracture by the fluid entails the occurence of a large part of the seismicity.

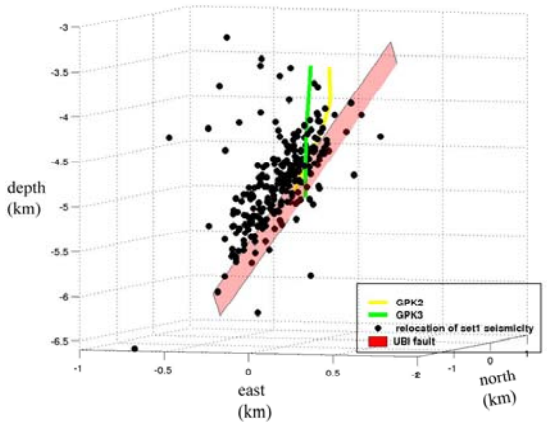

Figure 4 The seismicity relocated in the 3D model velocity determined by the tomography. This seismicity is located just above the fracture imaged by UBI (pink-red plane) . The well GPK3 is in green and GPK2 in yellow.

Acknowledgment: this work is part of Jean Charléty Ph.D. thesis supported by ADEME.(Agence de l'Environnement et de la maitrise de l'énergie). We thank also the EEIG "Heat Mining" for having given us the hydraulic data. We also thank all the people who worked for maintaining the permanent network: Hervé Blumentritt, Michel Frogneux, Jacki Sahr.

REFERENCES

Benderitter, Y., and Elsass, P. (1995), "Structural control of deep fluid circulation at the Soultz HDR site, France: a review", *Geotherm. Sci. Technol.*, vol **4**, 227-237.

Cuenot, N., Dorbath, C., Dorbath, L., (2005), "Analysis of the microseismicity induced by fluid injections at the Hot Dry Rock site of Soultz-sous-Forêts (Alsace, France): implications for the characterization of the geothermal reservoir properties.", *Pure and Applied Geophysics*, accepted

Dezayes, Ch., Genter, A., Homeier, G., Degouy, M., Stein, G., (2003), "Geological study of GPK3 HFR borehole (Soultz-sous-Forêts, France)", *BRGM/RP-52311-FR*, 128 p.

Helm, J.A. (1996), "The natural seismic hazard and induced seismicity of the European Hot Dry Rock geothermal energy project at Soultz-sous-Forêts (Bas-Rhin, France)", *Thèse de Doctorat, Ecole et Observatoire des Sciences de la Terre, Université Louis Pasteur (Strasbourg I)*, 197 p.

Ito, H., De Vilbiss, J. and Nur, A., (1979), "Compressional and shear waves in saturated rock

during water-steam transition", *Journal of Geophysical Research*, vol **84**, n° B9, 4731-4735.

Klee, G., and Rummel, F. (1993), "Hydrofrac stress data for the European HDR research project test site Soultz-sous-Forêts", *Int. J. Rock Mech. Min. Sci. & Geomech. Abstr*., vol **30**, 973-976.

Leonard, M., Kennett, B.L.N., (1999), " Multi-component autoregressive techniques for the analysis of seismograms", *Physics of the earth and Planetary Interiors*, vol. **113**, 247-263.

Nur, A., and Simmons, G. (1969a), "The effect of saturation on velocity in low porosity rocks", *Earth Planet. Sci. Lett.* , vol **7**., 183-193

Rummel, F., and Baumgärtner, J. (1991), "Hydraulic fracturing stress measurements in the GPK1 borehole, Soultz-sous-Forêts", *Geotherm. Sci. Technol.*, vol **3**, 119-148.

Tenzer, H., Mastin, L., and Heinemann, B. (1991), "Determination of planar discontinuities and borehole geometry in the crystalline rock of borehole GPK1 at Soultz-sous-Forêts", *Geotherm. Sci. Technol.*, vol **3**, 31-67.

Thurber, C.H., (1983), "Earthquake locations and three-dimensional crustal structure in the Coyote Lake area, central California", *Journal of Geophysical Research*, vol **88**, 8226-8236.

Waldhauser, F., (2001), "hypoDD: a computer program to compute douoble difference hypocenter locations", *U.S. Geological Survey Open File Report 01-113*, 25 p.

Wyllie, M.R., Gregory, A.R., and Gardner, L.W. (1956), Elastic wave velocities in heterogeneous and porous media, *Geophysics*, vol **21**, 41-70.

Wyllie, M.R., Gregory, A.R., and Gardner, L.W. (1958), "An experimental investigation of factors affecting elastic wave velocities in porous media", *Geophysics*, vol ***23***, 459-493.

Zhang, H. and Thurber, C.H., (2003), "Double-difference tomography: The method and its application to the Hayward fault, California", *Bulletin of the Seismological Society of America*, vol.**93**, n° 5, 1875-1889.